GSEOPTICS2024
Nov 22-23, 2024 | Dubai, UAE

Anna T. Kurzych

Leszek R. Jaroszewicz

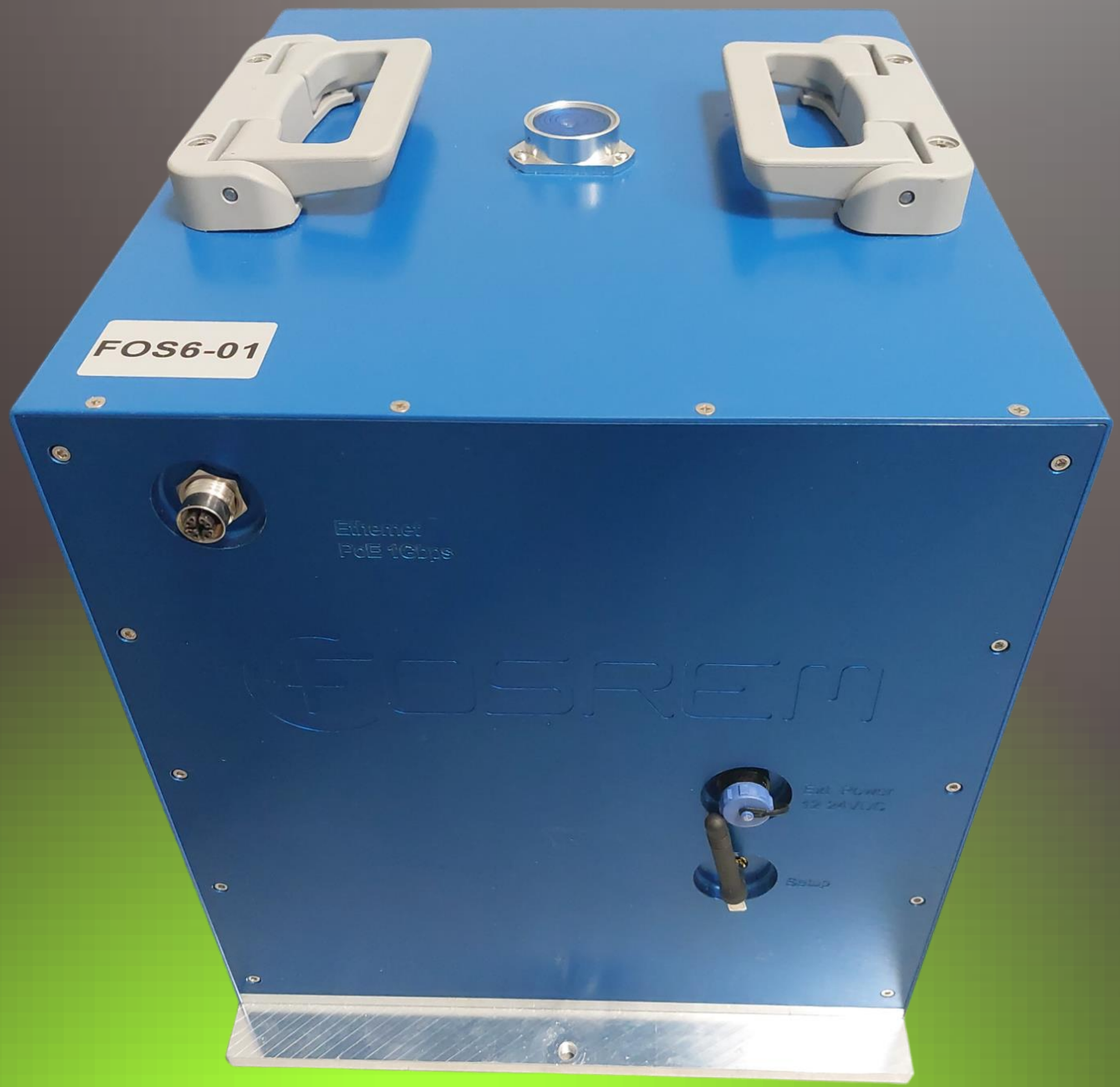

Rotational Seismology Achievements from an Instrumentation Point of View – How precise is precise enough?

Military Univeristy of Technology, Institute of Appied Physics, Warsaw, Poland
Elproma Electronics Ltd., Czosnow, Poland

Rotational seismology

2006

The International Working Group on Rotational Seismology (IWGoRS, www.rotational-seismology.org) was initiated during a meeting organized by the United States Geological Survey in Menlo Park

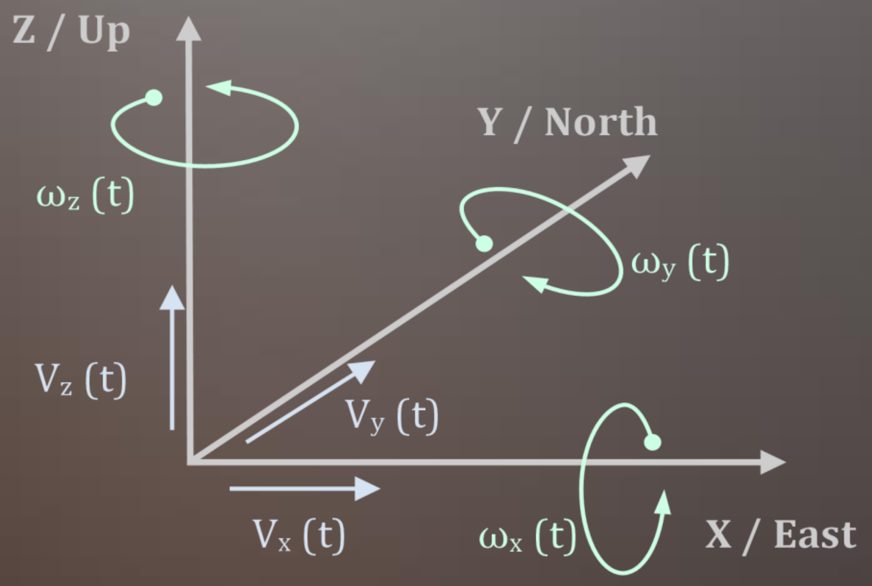

2009

RS - a new, emerging field for the study of all aspects of rotational ground motion induced by earthquakes, explosions, and ambient vibrations [Lee et al. BSSA, 2009, 99, 945-957]

Engineering application

seismic behaviour of irregular and complex civil structures, [Trifunac, BSSA, 99, (2009), 968-97; Mustafa, InTech, 2015], Structural Health Monitoring [Bonkowski and Z. Zembaty, WCEE2024, Milan, Italy, 2024]

Seismological application

broadband seismology [Igel et al., Geophys. J. Int., 168(1), (2006), 182–197], strong-motion seismology [Anderson, 2003, Chap. 57, 937-965], earthquake physics [Teisseyre et al. Springer, 2006; Springer, 2008], seismic hazards [McGuire, Earthq. Eng. Struct. D., 37, (2008), 329–338], seismotectonics [www.geophysik.uni-uenchen.de/~igel/Lectures /Sedi/sedi_te ctonics.ppt], geodesy [Carey, Expanding Earth Symposium, (1983), 365-372], physicists using Earth-based observatories for detecting gravitational waves [Ju et al., Rep. Prog. Phys., 63, (2000), 1317–1427; Lantz et al., BSSA, 99, (2009), 980-989]

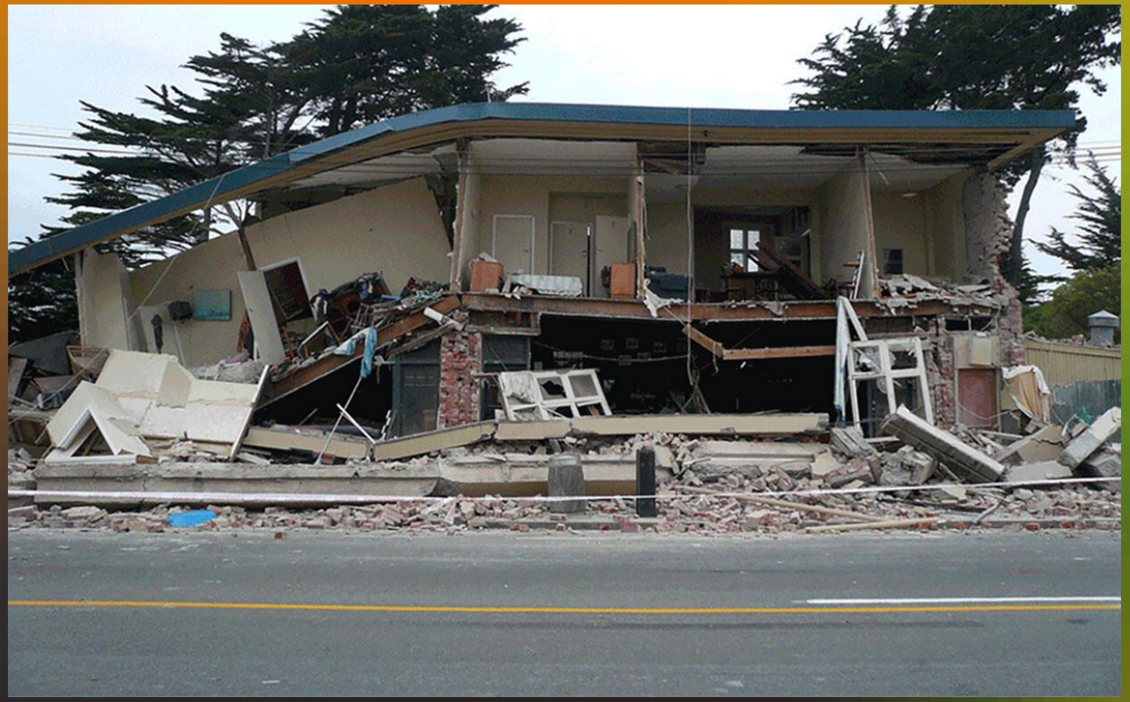

Building damanged by the February 2011 earthquake in Christchurch, New Zealand [https://www.usgs.gov/media/images/earthquake-damaged-building -damaged-building]

A view shows damage at an old mosque in the historic city of Marrakech, following a powerful earthquake in Morocco, September 9, 2023 [https://edition.cnn.com/2023/09/10/africa/mosque-earthquake-damage-marrakech-intl/index.html]

Seismological application

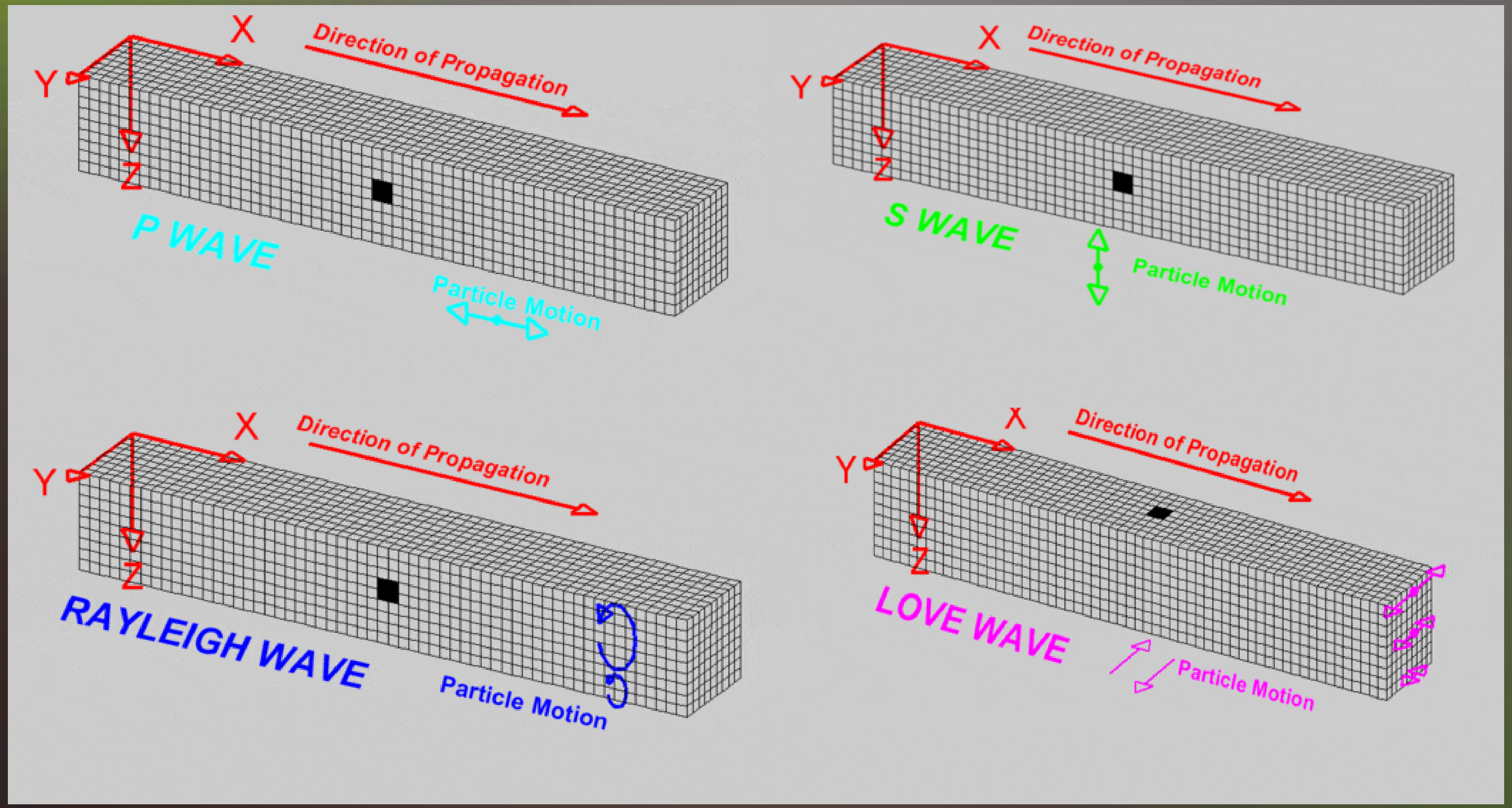

[https://www.geometrics.com/support/different-types-of-seismic-waves/]

Energy generated during an earthquake propagates not only in a form of linear motions but also in rotational ones.
Earthquakes are undoubtedly one of the most complex phenomena and it is hard to entirely reflect their complexity in theoretical models

Examples of rotations observed in downtown L'Aquila
[Castellano, C., *Boll. Geofis. Teor. Appl.* **2011**, *53*, 299–312. https://doi.org/10.4430/bgta0045]

Engineering application

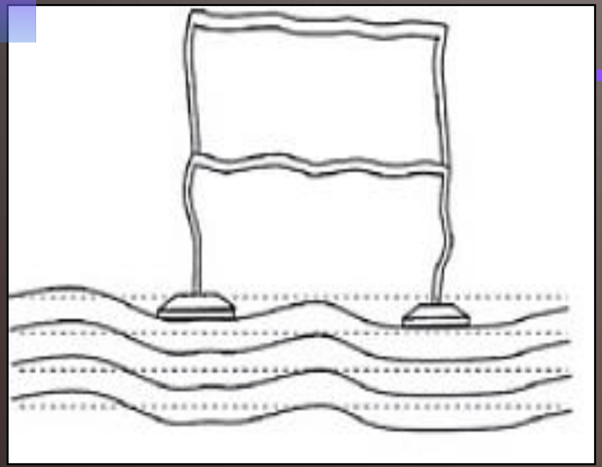

High frequency content

- **Local vibration of beams and columns**
- Meaningless motion of the building center of mass

Damages in building after September 21, 1999, a strong earthquake of 7.3 in the central part of Taiwan, presented in 921 Earthquake Museum of Taiwan

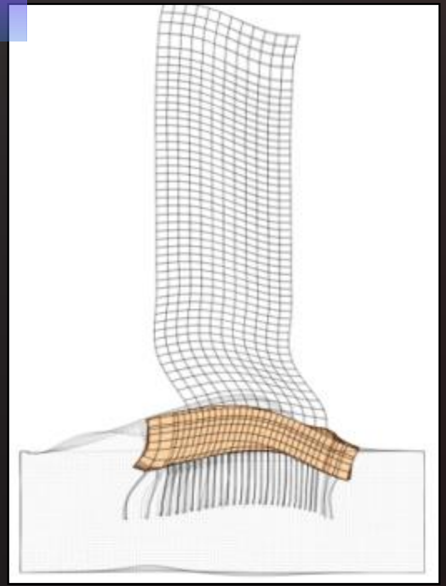

Snapshot of the model of displacement response to an incident plane P-wave half sine displacement pulse with 45° incident angle (view from South) [Todorovska M. I., WCEE2024 Processing, 2024]

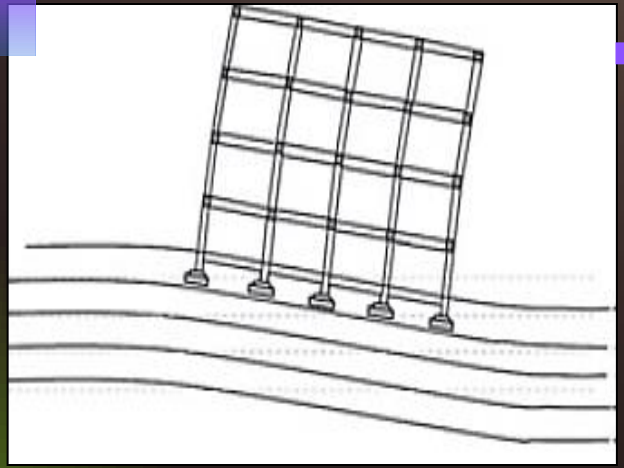

[Castellani, Guidotti, 2nd Workshop of IWGoRS Masaryk 's College Prague, (2010)]

Low frequency content

- Higher stress in structural element
- **Overturning moment**
- Horizontal displacement of the center of mass

Example of an overall rotation of the base of the structure with an overturning motion during 1999 Kocaeli earthquake, Turkey [Bozzoni, F. et al., *Bull. Earthq. Eng.* **2021**, *19*, 4719–4744]

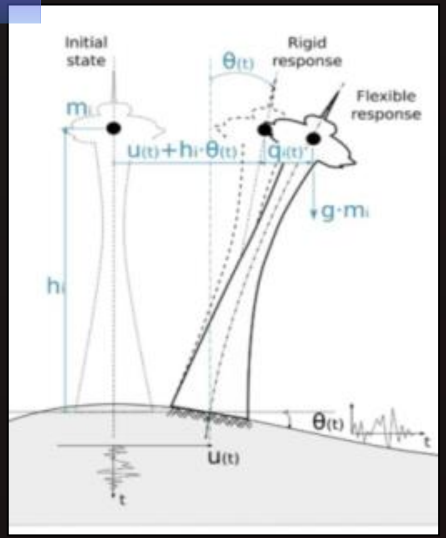

A slender structure under horizontal-rocking ground vibrations [Bońkowski et al., Engineering Structures 155, 387-393, 2018]

Classification of rotation measurements

Strong-motion of the order of tens of μrad/s and more	Rotation with a very low amplitude of the order of tens of 10^{-7} rad/s or less
• Rotational motions of the ground in the near-source field • Rotation associated with volcanic eruptions • Rotation recorded during chemical explosions • Rotation connected with engineering seismology	• Rotation measurements of teleseismic waves • Measurements of rotation related to the physics of seismological interactions • Rotation studies in a micromorphic medium

The frequency range can reach 10^{-4} Hz to 100 Hz;

Indirect rotation research by numerical conversion

Y	Ref.	F [Hz]	ES	M_w	R [km]	PGV_h [m/s]	PGV_v [m/s]	$PG\omega_z$ * [μrad]	$PG\omega_z$ [mrad/s]	$PG\omega_x$ * [μrad]	$PG\omega_x$ [mrad/s]	$PG\omega_y$ * [μrad]	$PG\omega_y$ [mrad/s]
1982	Bouchon and Aki		strike-slip fault	6.6	1	1/1.6	-	200/ 300	1.2/1.5	700/800		-	
2003	Huang	<1.0	The 1999 Chi-Chi, Taiwan earthquake (thrust fault)	7.7	6	0.33	0.50	171	0.385	44	0.126	177	0.331
2008	Spudich and Fletcher	<3.6	2004 Parkfield, California, earthquake and aftershocks (strike-slip fault)	6.0	8.8	0.25	-	88.1	1.09	68.9	0.925	-	-
				4.7	14.0	0.013		4.69	0.0944	4.74	0.0926		
				5.1	14.4	0.060		20	0.446	0.177	0.372		
				4.9	18.3	0.027		13.6	0.247	9.73	0.215		
2009	Stupazzini, et al.	<2	valley of Grenoble, French (strike-slip)	6.0	0.02-0.90	0.4	0.3	1 690	8.24	4000	8.66	1310	0.6
2009	Wang, et al.	<0.5	Newport-Inglewood strike-slip	7.0	<80	-	-	-	3.00 *		0.350 *	-	0.6 *
2019	Cao and Mavroeidis		hypothetical strike-slip earthquake	6 6.47.27. 6	1-50	<0.72	<0.24	69.2-194.2		16.9-94.3	-	22.7-98.5	-
			dip-slip earthquake	6 6.4 6.87.27. 6	1-50	<0.66	<0.93	54.1-144.3		117.9-421.9	-	144.2-325.3	-
2021	Cao and Mavroeidis	<1.0	Izmit earthquake 1999	7.5	1-50	0.11-0.63 *	0.03-0.19 *	52.6-155 *	-	6.2-43.3 *	-	10.7-47.4 *	-
			2004 Parkfield	6.0	1-50	0.005-0.23 *	0.003-0.045 *	5.6-35.5 *		2.5-23.1 *		1.4-30.7 *	
			1979 Imperial Valley	6.5	1-50	0.06-0.83 *	0.007-0.13 *	21-178 *		9.7-89 *		3.9-29.8 *	

Parameters of the rotation (selected maximum value) obtained indirectly by numerical analysis. Legend: Y – year of publication, Ref. – reference, ES – earthquake source mechanism, M_w - magnitude, R – epicentral distance, PGV_h – peak value of horizontal ground velocity, PGV_v – peak value of vertical ground velocity, $PG\omega_{z,x,y}$ – peak value of rotational velocity around the particular axis.

* $PG_{\omega z,x,y}$ – ground rotation around the particular axis depending on the distance

[Kurzych, A.T. et al., *Sensors* **2024**, *24*, 7003]

Bouchon and Aki used the discrete wavenumber representation method

Huang presented calculated rotations from translational velocities by numerically integrating accelerograms from a dense acceleration system

Spudich & Fletcher provides an estimate of the rotation of the September 28, 2004, mainshock in Parkfield, California

Stupazzini et al. simulated the rotational wave field 3D numerical modeling

Wang et al. simulated using a finite-difference method over a frequency range of up to 0.5 Hz. The analysis showed that the variability of the hypocenter leads to significant changes in the ground rotation speed.

Cao and Mavroeidis finite differential translational motions generated at very closely spaced stations

Rotation effects recordings during natural earthquakes

Y	Ref.	ES	Sensor	M_w	R [km]	PGV_h [mm/s]	PGV_v [mm/s]	$PG\omega_z$ [mrad/s]	$PG\omega_x$ [mrad/s]	$PG\omega_y$ [mrad/s]
1998, 2006	Takeo	strike-slip fault, 1997	Systron Donner triaxial gyro sensor	5.7	3.3	290	500	3.3	26	5.9
				5.3	3.3	200	100	8.1	27	30
2009	Takeo	seismic swarm activities at offshore Ito, Japan, 1998	Systron Donner triaxial gyro sensor	5.0	5.6	100	60	3	6	8
				3.6	5.9	6	2	0.2	1	1
				2.4	4.9	6	0.3	0.03	0.2	0.2
2009	Liu et al.	local earthquakes at the HGSD station in Eastern Taiwan	R-1	5.1	51	-	-	0.63	~0.4	~0.3
				2.5-6.63	14.3-260.4	-	-	0.004-0.63	-	-
2010	Brokešová and Málek	earthquake swarm in Western Bohemia, 2008	Rotaphone 3DOF	2.2	4.4	400	-	0.15	-	-
2013	Brokešová and Málek	an earthquake recorded at the station Sergoula, Greece	6 DOF Rotaphone	4.3	5	4.5	9	~0.4	~0.8	~0.7
2016	Yin et al.	215 events at The Garner Valley Downhole Array is in California, 2008- 2014	R-1	3.0-7.2	14-207	-	-	0.006-0.453	-	0.004-0.7
2017	Jaroszewicz et al.	local earthquake, Jarocin, Poland	TAPS	3.8	200	-	-	0.005	-	-
			AFORS					0.039		
2018	Ringler et al.	local earthquake	Two SMHD (ATA)	4.2	0.5	22.1	11	1.12/0.85	-	2.11/1.86
		local earthquake		2.8	≤220	-	-	~0.0005	~0.00025	~0.00025
		155 local earthquake		≥2.0	≤220			0.0002-2	0.0002-2	0.0002-2
2020	Wasserman n et al.	volcano-tectonic earthquake	BlueSeis-3A	5.3	1.5	2	1	2.4	2.5	2.4
2022	Wasserman n et al.	Stromboli volcano, Italy activity	BlueSeis-3A	-	-	<0.01	<0.02	<0.0005	<0.001	<0.001

Parameters of the rotation recordings generated by natural earthquakes. Legend: Y – the year of publication, Ref. – reference, ES – earthquake source, M_w - magnitude, R – epicentral distance, PGV_h – peak value of horizontal ground velocity, PGV_v – peak value of vertical ground velocity, $PG\omega_{z,x,y}$ - peak value of rotational velocity about a particular axis

[Kurzych, A.T. et al., *Sensors* **2024**, *24*, 7003]

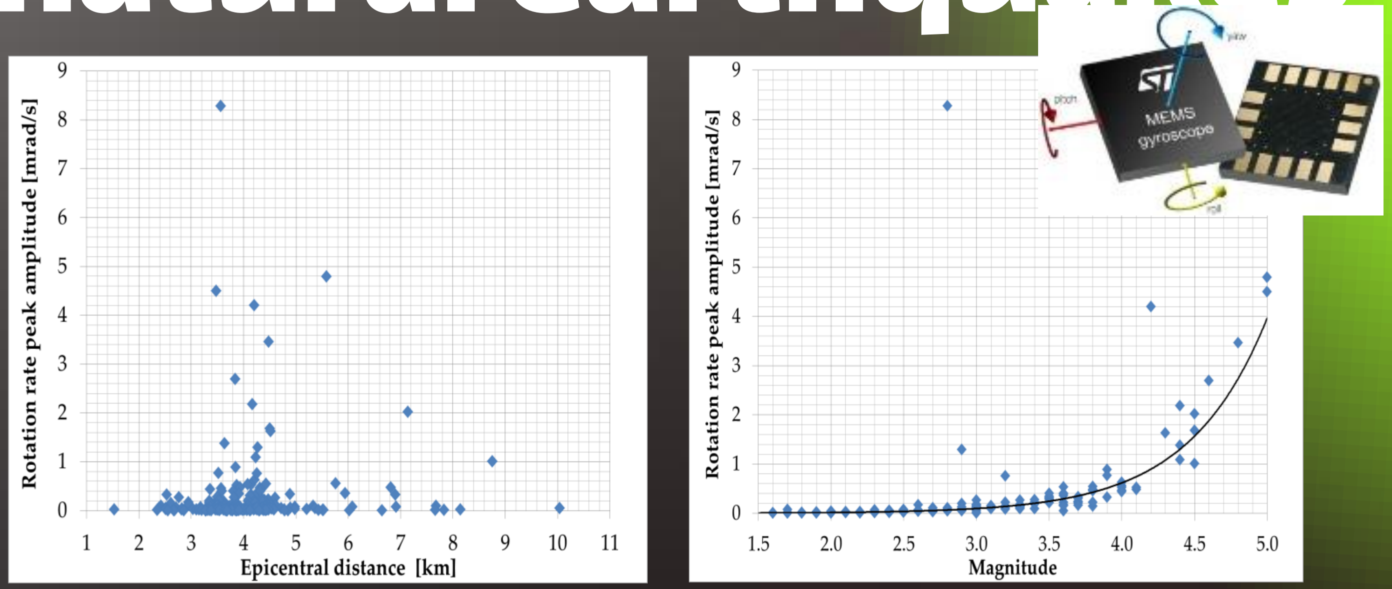

Takeo – 3-axial Gyro (Systron Donner)

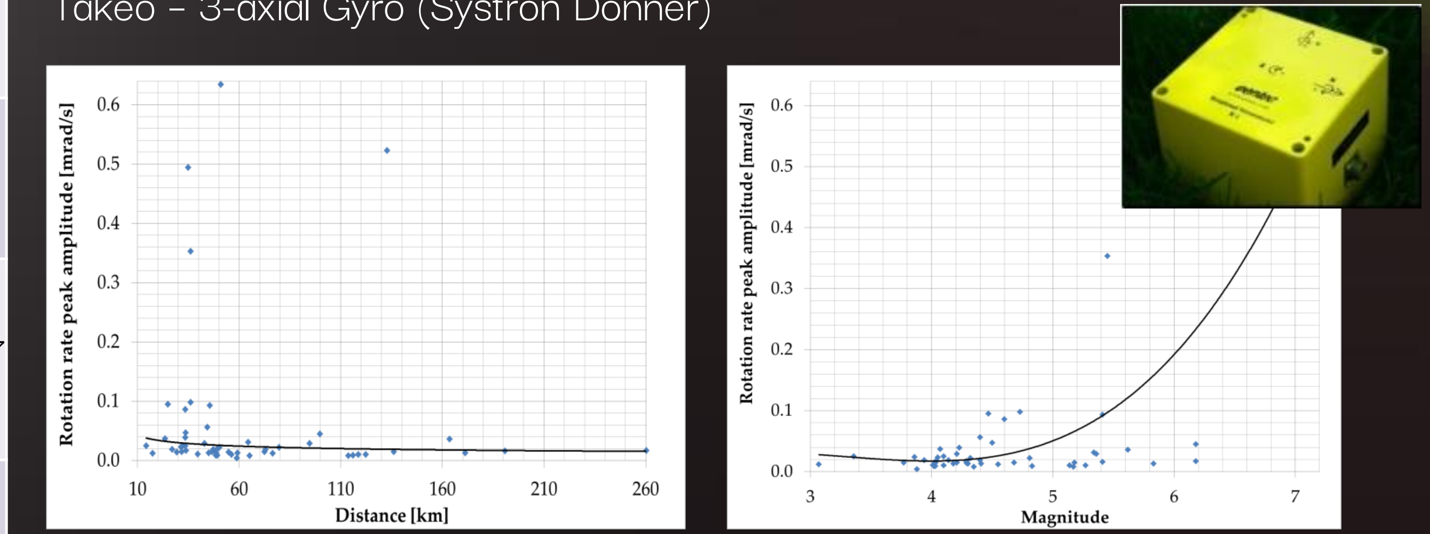

Liu, Yin – R-1 (Eentec)

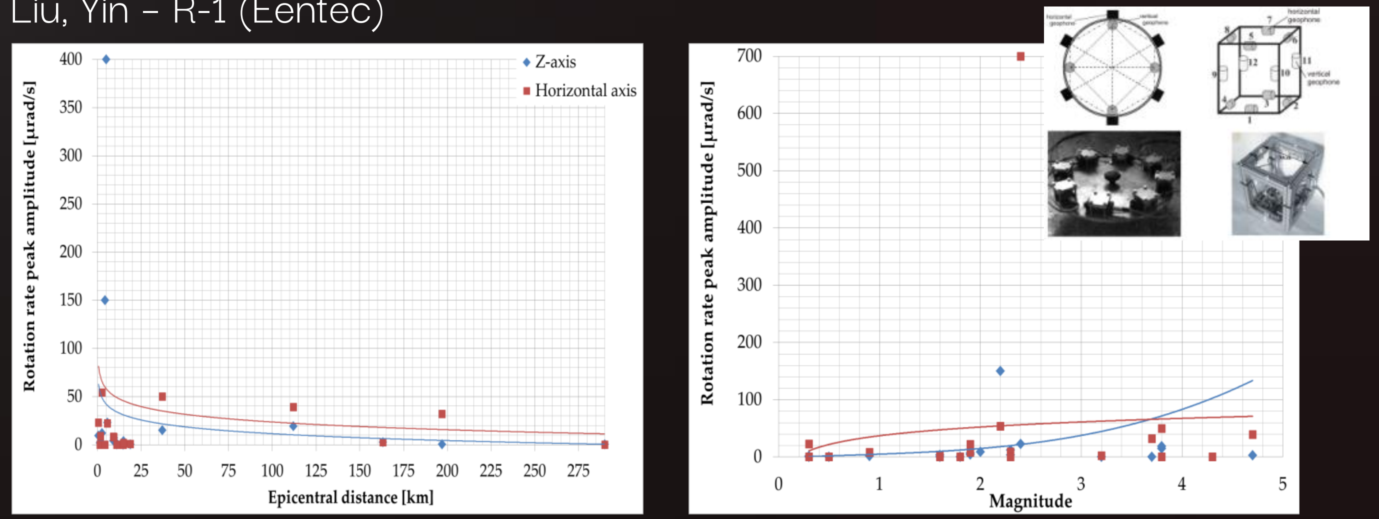

Brokesova – 3DOF, 6DOF Rotaphone (Czech Republic)

Recordings associated with artificial explosions

Y	Ref.	VS	Sensor	R [km]	PGω_z [mrad/s]	PGω_x [mrad/s]	PGω_y [mrad/s]
1994	Nigbor	1 kT chemical explosion at the Nevada Test Site	QRS11 (Systron Donner)	1	24	38	-
2009	Wasserman et al.	Demolition blast of building in Munich, Germany	R-1, eentec	0.2	0.02	0.008	0.5
2009	Lin et al.	3000 kg explosives, TAIGER experiment, Tawian	R-1, eentec	0.2539-0.6082	0.268-0.966	0.370-2.741	0.627-2.524
		750 kg explosives, TAIGER experiment, Tawian			0.301-0.563	0.235-1.750	0.394-1.185
2013	Brokešová and Málek	medium-size quarry blast, 3044 kg explosive, Czech Republic	6 DOF Rotaphone	0.362	~1	~4.5	~2
2018	Barak et al.	Ignition of Betsy gun at Silver Lake, California	METR-03	<1	-	<0.1	<0.2
2019	Kurzych et al. Teisseyre et al.	Digging shafts with the multiple blasts technique, Książ, Poland	FOSREM, TAPS, RS.LQ-RP/P	0.075	0.05-1	-	-
2021	Bernauer et al. Kurzych et al.	500 g explosive, Fürstenfeldbruck, Germany	BlueSeis-3A, FOSREM, ROMY, Rotaphone-CY, FARO, PHINS, Quadrans, MEMS gyroscopes (Horizon, Gladiator)	~0.05	~0.5 (BlueSeis-3A) ~1 (FOS5-01) ~0.5 (FOS5-02) <0.5 * (BlueSeis-3A) ~0.005 * (ROMY) <0.02 * (FARO) <0.025 *(FOS5) ~0.025 * (PHINS) <0.025 *(Quadrans) <0.05 *(Rotaphone)	<0.1 * (BlueSeis-3A) <0.15 * (PHINS) < 0.1 * (Quadrans) <0.09 * (Rotaphone)	~0.1-0.15 (BlueSeis-3A) <0.15 (PHINS) <0.15 (Rotaphone) <0.15 * (BlueSeis-3A) ~0.15 * (PHINS) <0.15 *(Quadrans) <0.15 *(Rotaphone)
		VibroSeis truck, Fürstenfeldbruck, Germany	FOS5-1	0.096	0.0177	-	-
				0.105	0.0252		
				0.113	0.0386		
				0.121	0.0158		
				0.130	0.0156		
				0.138	0.0141		
2021	Cao et al.	near field explosion, China	RotSensor3C	0.150	~11	~11	~16
2022	Brokešová and Málek	medium-size blast at the Klecany quarry, Czech Republic	Rotaphone, R-1, ADR (array-derived-rotation)	0.240	~0.05 (Rotaphone) ~0.01 (R-1) ~0.05 (ADR)	~0.25(Rotaphone) ~0.1 (R-1) ~0.25 (ADR)	~0.15 (Rotaphone) ~0.03 (R-1) ~0.1 (ADR)
					~0.05 (Rotaphone) ~0.03 (R-1) ~0.06 (ADR)	~0.25 (Rotaphone) ~0.2 (R-1) ~0.22 (ADR)	~0.2 (Rotaphone) ~0.08 (R-1) ~0.1 (ADR)

[Kurzych, A.T. et al., *Sensors* **2024**, *24*, 7003]

[https://www.youtube.com/watch?v=gt_FkmalX9U]

"Rotation and strain in Seismology: A comparative Sensor Test" gathered more than 40 sensors in the Geophysical Observatory Fürstenfeldbruck, Germany, from 18-22 November 2019.

Wassermann used R-1 rotational sensor to record rotation generated by the demolition blast of a 50 m high building in Munich, Germany, at a distance of about 250 m.

Barak et al. recorded rotation generated by the ignition of the Betsy gun was the source of seismic events in Silver Lake, CA, USA. The recorded signal around the Y-component (max. 0.2 mrad/s) of rotation was higher than the maximum amplitude of the signal around the X-component, which the authors expected according to the rotational deformation caused by the Rayleigh wave in the analysed survey

Recordings associated with mining activity

Y	Ref.	F [Hz]	VS	Sensor	M_w	R [km]	PGV_h [mm/s]	PGV_v [mm/s]	$PG\omega_z$ [µrad/s]	$PG\omega_x$ [µrad/s]	$PG\omega_y$ [µrad/s]
2014	Kurzych et al.	0.83-106.15	mining activity, Lubin, Poland, 2011-2013	AFORS	2.3-3.3	70	-	-	6 /60	-	-
			earthquake Honshu, Japan, 2011		9	8800			15		
2015	Brokešová and Málek	2-60	geodynamically active region, West Bohemia/Vogtland, 2012, (band-pass filtered 2-24)	Rotaphone 6DOF	2	0.7	0.081	0.02	4	5.7	4
			active rift, Gulf of Corinth, Greece, 2012 (band-pass filtered 1-14)		2.4	6.3	0.326	0.06	10	15	25
			Microearthquake, rifting and volcanic activity in South Iceland, 2014 (band-pass filtered 1-14)		2.3	14.9	0.05	0.025	3.3	1	2.5
2016	Zembaty et al.	0.05-20	mining exploration monitoring, USCB, Poland	R-1	2.6	0.943	20.3	-	491	513	527
					2.5	1.203	8.3		514	425	298
					2.2	0.973	13.8		430	276	500
2019	Kurzych et al.	DC-328.12	seismic shocks induced by the exploitation of copper ore, Książ, Poland, 2017-2018	FOSREM	-	70	-	-	1-20	-	-
2020	Fuławka et al.	0.05-20	tremor in the near-wave field, Rudna-I shaft, Poland, 2019	R-1	-	<7	0.01-4	0.01-4	few µrad/s up to 195 mrad/s *		
			monitoring of the tailing pond, Poland, 2019		-	2.3-8	0.01-4	0.01-4			
2021	Jaroszewicz et al.	DC-1000	mining-induced events, coalmine "Ignacy", Rybnik, Poland, 2021	FOSERM	-	-	-	-	51.8 (FOS5-01) 60.8 (FOS5-02)	-	

[Kurzych, A.T. et al., *Sensors* **2024**, *24*, 7003]

Zembaty et al. collected 51 records of ground rotation from a surface measuring station located in the mining area of the Ziemowit coal mine. The maximum value of the recorded rotational velocity about the north-south axis equals 0.527 mrad/s, and it corresponds to a maximum acceleration equal to 32.348 mrad/s2 for the event with a magnitude of 2.6.

Fuławka et al. focused on Zelazny Most–one the biggest flotation tailing ponds worldwide and the Rudna-I mining shaft. The maximum rotational velocity of the seismic wave reached the value of 195 mrad/s and was caused by a seismic tremor with the energy of $3.6 \cdot 10^7$ J located at a distance of 1.550 km from the measuring post.

Kurzych et al. presented regional seismic mining events of a magnitude range of 2.3-3.3, which occurred in the Lubin area, Poland, with the maximum rotational velocity amplitude reaching 60 µrad/s recorded by AFORS-1. In the period of 12 January 2017-18 January 2018, two FOSREMs recorded two types of signals around the Z-axis–torsion and tilt, in the frequency range DC-10.25 Hz

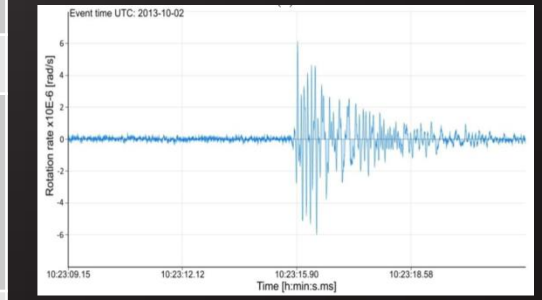

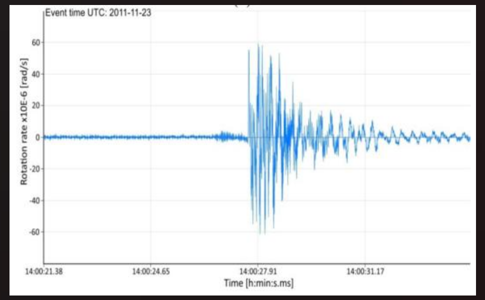

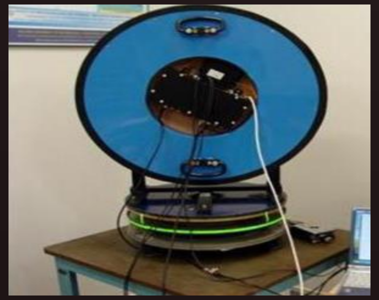

A. Kurzych et al., Sensors, 14, (2014), 5459-5469

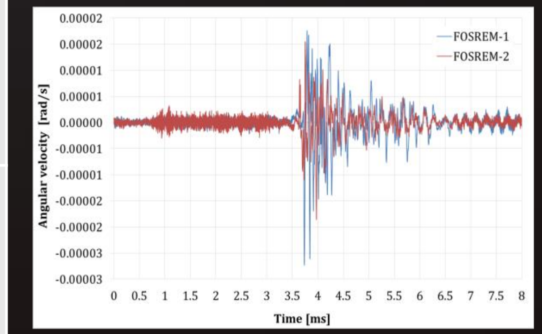

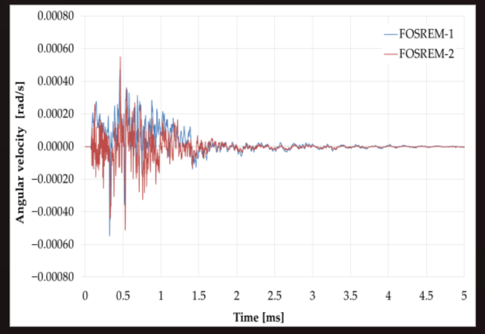

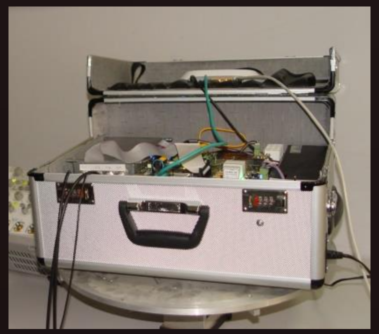

Recordings associated with teleseismic waves

Y	Ref.	ES	Sensor	M_w	R [km]	PGV_h [m/s]	$PG\omega_z$ [nrad/s]	$PG\omega_x$ [nrad/s]	$PG\omega_y$ [nrad/s]
2000	Pancha et al.	New Ireland earthquake, 1999	C-II, G0	7.0	~4700	-	10 (C-II)	5 (G0)	-
		Vanuatu earthquake, 1999	C-II	7.3	~3500		8	-	
2005	Igel et al.	Thrust earthquake Japan	G-ring	8.1	~8830		~35		
2007	Igel et al.	from local event, Germany to Great Andaman earthquake	G-ring	5-9	370-12,700	-	~0.10 -40	-	-
2009	Schreiber et al.	Earthquake Kamachatka, 2006	GEOsensor	7.6	~6500	5197	~10	-	-
		Earthquake Mexico, 2006		5.4	~2000	4646	~5		
		Earthquake California, 2007		3.6	~200	8670	~16		
		Earthquake California, 2007		3.9	~250	14,512	~30		
2011	Lin et al.	Earthquake in Wenchuan Sichuan, China	R-1	7.9	1948	<0.01	-	10,000	10,000
2012	Belfi et al.	Earthquake in Japan, 2011	G-Pisa	9.0	-	-	~60	-	-
2017	Ross et al.	earthquake Papua New Guinea, 2016	beam rotation sensor BRS	7.9	-	$\sim 150 \times 10^{-6}$	-		~30 *
		earthquake Vanuatu, 2016		6.7		$\sim 6 \times 10^{-6}$			~2 *
		earthquake New Caledonia, 2016		7.2		$\sim 40 \times 10^{-6}$			~10 *
		earthquake north of Ascension Island, 2016		7.1		$\sim 15 \times 10^{-6}$			~4.5 *
		earthquake New Zealand, 2016		7.8		$\sim 200 \times 10^{-6}$			~60 *
		earthquake of Panguna, Papua New Guinea, 2017		7.9		$\sim 150 \times 10^{-6}$			~30 *
2018	Simonelli et al.	Series of earthquakes in Italy, 2016	GINGERino	3.5-5.9	38-77	-	~600-17,000	-	-
2020	Sollberger et al.	Earthquake Gulf of Alaska, 2018	ROMY	7.9	-	-	~6	~8	~4
2021	Igel et al.	Papua New Guinea earthquake, 2019	ROMY	7.6	14,000	-	~8.5	~9	-
		Turkey earthquake, 2019		5.7	1500		~5	~9	
		Austria earthquake, 2018		3.8	144		~18.9	~18	

- strong earthquakes
- extremly distance R
- extremely low PGw (nrad/s) amplitude

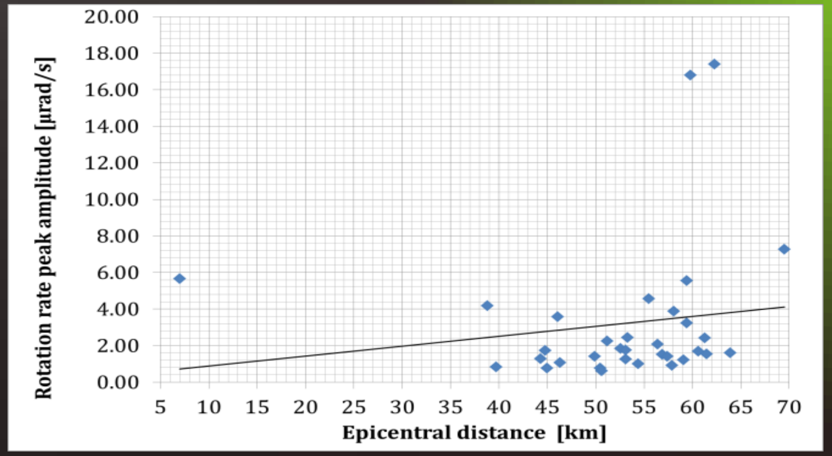

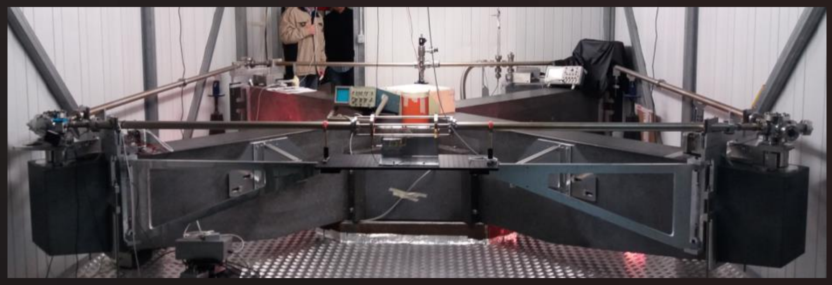

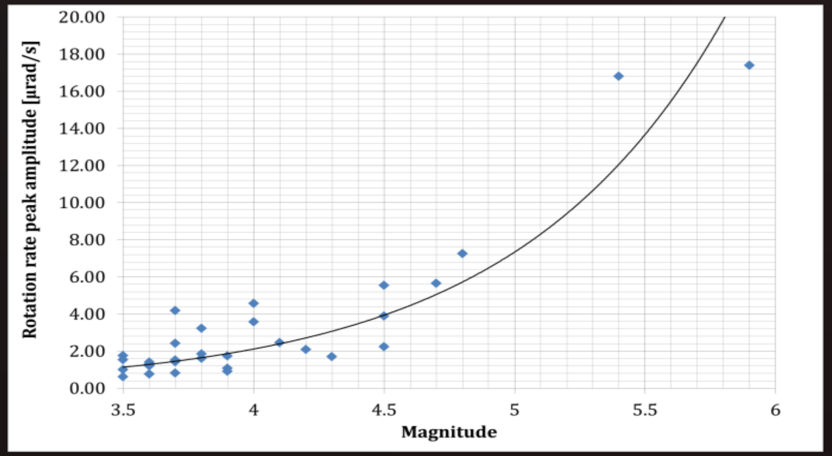

GINGERino results
Peak values of rotation rate around the vertical axis for 33 presented events ranged from $6.14 \cdot 10^{-7}$ to $1.74 \cdot 10^{-5}$ rad/s
[A. Simonelli, PhD Dissertation, Ludwig-Maximilians-Universitat Munchen, Munchen, 2018]

[Kurzych, A.T. et al., *Sensors* **2024**, *24*, 7003]

Requirements

Insensitivity to linear motion
Mobility, stability with respect to environmental conditions, including changes of temperature
Independent power supply
Dynamic range 10^{-8} - 10 rad/s
Frequency band 0.01 - 100 Hz
Power consumption 5 – 8 W
Thermal stability <0,1% / °C
Calibration – in situ (permanently)

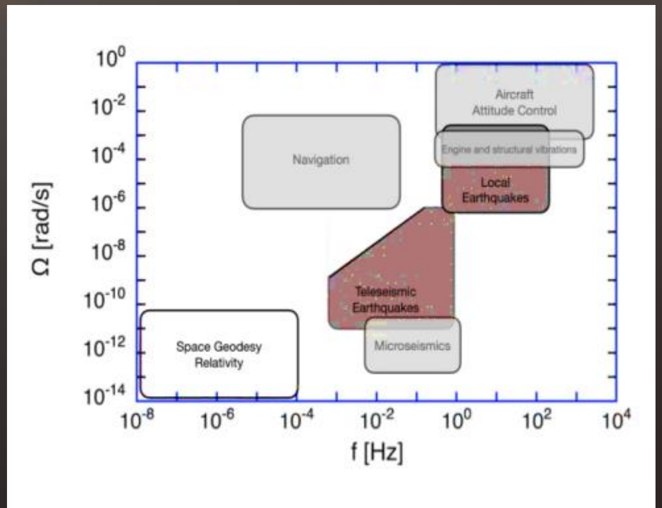

[Schreiber U, Kodet J, WCEE Processing, Milan, Italy 2024]

Engineering application

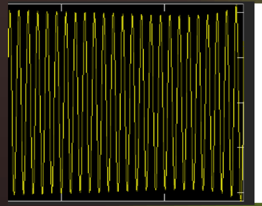

signal amplitude:
up to 10 rad/s

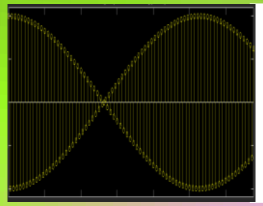

frequency: 0.01 Hz – 100 Hz

Seismological application

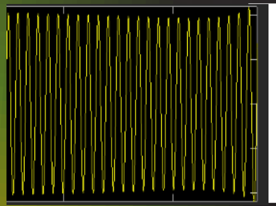

signal amplitude: from 10^{-7} rad/s,

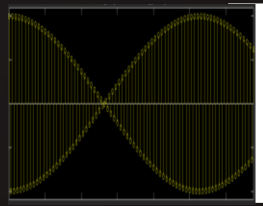

frequency: 0.01 Hz – 0.1 Hz

Group of sensors	Technology	Name of sensor	Picture	Manufacturer	Axial	Sensitivity [rad/s]	Max. rate [rad/s]	Dynamic range [dB]	Frequency range [Hz]	Sampling rate [Hz]	Operating temperature [oC]	Weight [kg]	Dimensions [L×W×H] [mm]
Mechanical	pendulum seismometers	TAPS		Institute of Geophysics PAS, Poland	uniaxial	$1\cdot10^{-7}$	0.1	120	0.7-50	100	−10-45	15	450x180x350
	geophones	3DOF		Charles University team, Prague, Czech Republic, led by Johana Brokešová		$1.67\cdot10^{-8}$	0.01	100	1–100	250	−20-40	4.5	250*×10
		6DOF			triaxial	$2.16\cdot10^{-9}$	0.287	120	2–60	250	−20-40	9.5	350×350×430
		D				$3.77\cdot10^{-9}$	0.0317	120	2–80	250	−40-70	15.3	445*×112
		CY				$0.042\cdot10^{-9}$	0.0317	120	1-100	250	−40-70	22	550*×500
	MEMS	G300D		Gladiator Technologies, Snoqualmie, USA		$2.97\cdot10^{-5}$	8.5	109	>600	10000	-50-85	0.19	25×25×15
		HZ1-200-100		Systron Donner Inertial, California, USA	uniaxial	$4.4\cdot10^{-4}$	3.49	77	> 60		-40-71	< 0.06	58.3×25.3×25.3
Electrochemical	MET	R-1		Eentec, Vilnius, Lithuania	triaxial	$1.2\cdot10^{-7}$	0.05	108	0.05-20		-15-55	~1	119×119×89
		R-2			triaxial	$6\cdot10^{-8}$	0.4	117	0.033-50		-15-55	1.5	120×120×100
		R-3	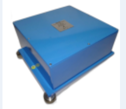		uniaxial	$2\cdot10^{-9}$	0.005	128	0.033-50		-15-55	3.5	250×250×100
Optical	RLG	G-ring		Geodetic Observatory Wettzell, Germany	uniaxial	$9\cdot10^{-11}$	1	280	0.003 - 10	4	Constant	No data	Area equal to 16 m^2
		ROMY		Geophysical Observatory Fürstenfeldbruck, Germany	triaxial	$(0.08 - 0.1)\cdot10^{-9}$			DC-1000	5000			tetrahedral-shaped 6 m side length
	FOG	BlueSeis-3A	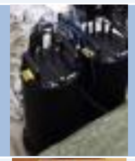	Exail (previously: iXblue), France	triaxial	$2\cdot10^{-8}$	0.1	135	0.001-100		-10-50	20	300×300×280
		FOS5		Military University of Technology, Poland	uniaxial	$9\cdot10^{-8}$	10	160	DC - 1000	200	-10-50	10	0.3*×0.09
		FORS		Elproma Electronics Ltd., Poland	triaxial	$35\cdot10^{-9}$	10	170	0.01-100	500	-10-50	20	360×300×29

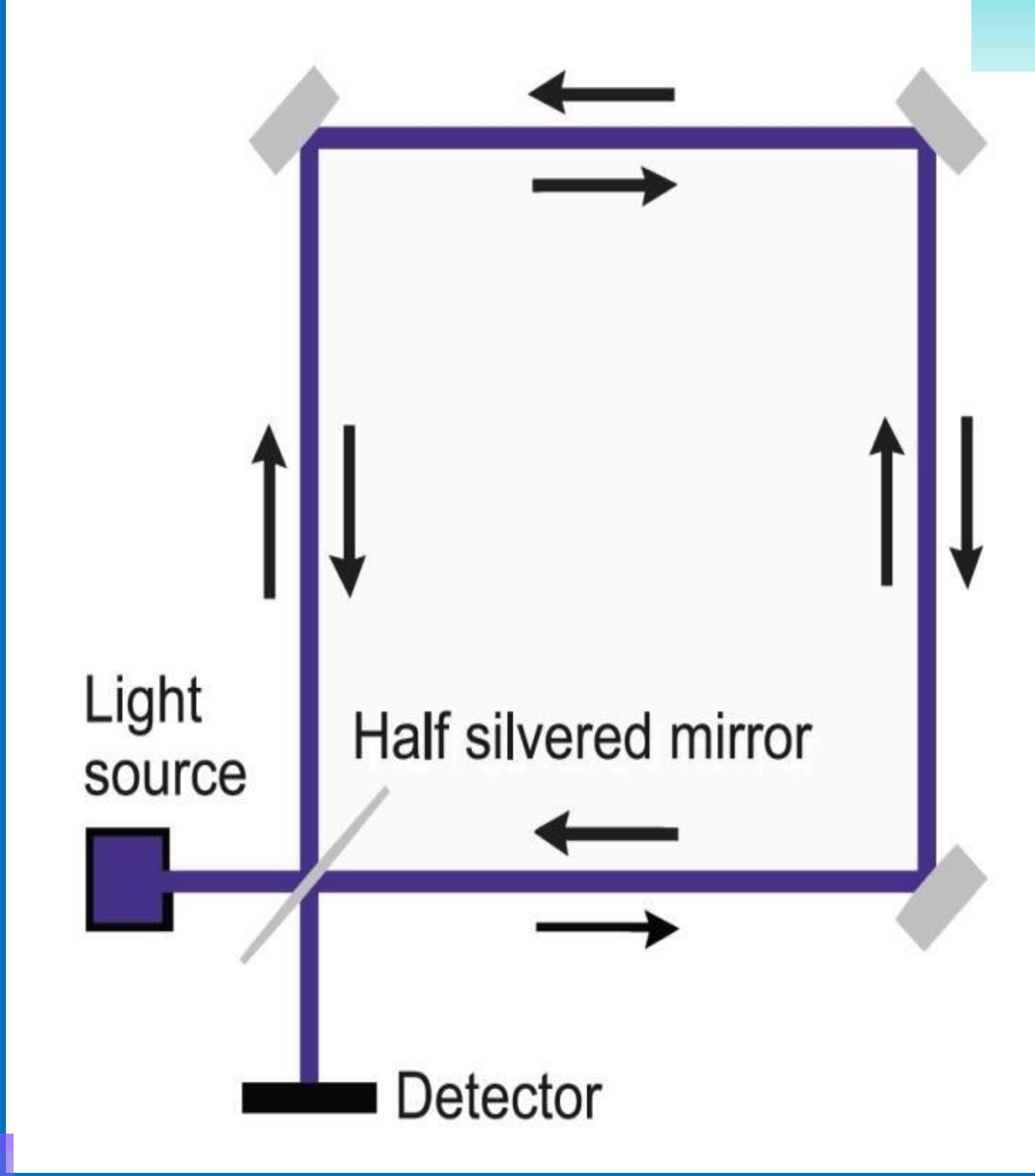

BACKGROUND

The direct utilization of the Sagnac effect

Sagnac effect shows the difference between phase of two beams propagating around closed optical path, in opposite direction when this path is rotating with rotational rate Ω. In a fiber-optic implementation the rotation rate Ω is expressed by induced phase shift $\Delta\varphi$ as:

$$\Omega = S_o \cdot \Delta\varphi = \frac{\lambda c}{4\pi RL} \cdot \Delta\varphi$$

L – length of the fiber in the sensor loop,
R – sensor loop radius,
λ – wavelength of used source,
c – velocity of the light in vacuum,
S_0 – the optical constant of interferometer

https://fosrem.eu

OPTICAL PART

generates the phase shift $\Delta\varphi$ proportional to the measured rotation rate Ω which is perpendicular to the sensor loop plane

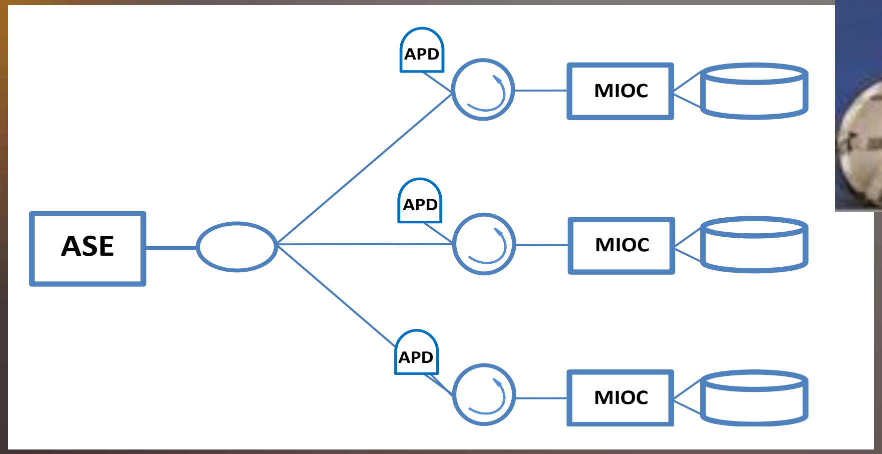

ELECTRONIC PART

enables to calculate and record information about rotational motions via digital closed-loop signal processing

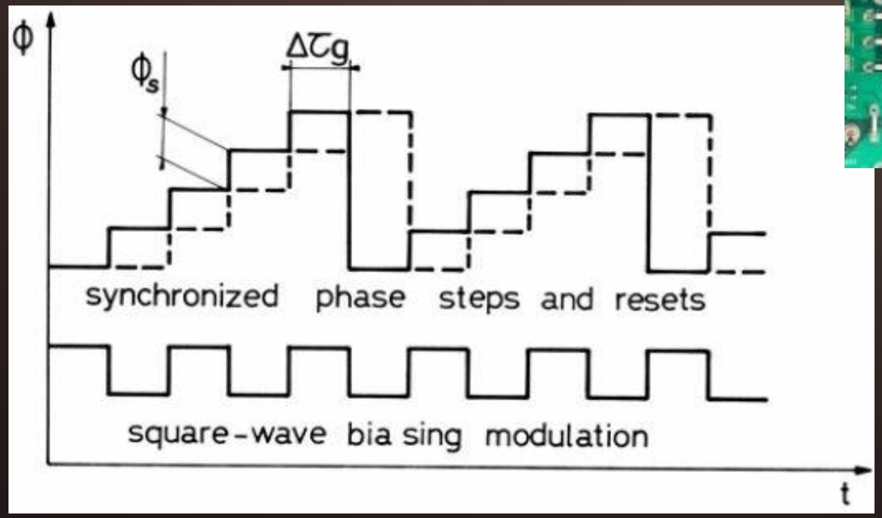

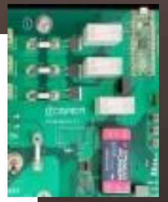

Fibre-Optic Seismograph

Allan Variance analysis

Theoretically

$$ARW = \frac{\sqrt{2}\lambda c}{2\pi DL}\sqrt{\frac{4kT}{R\eta^2P^2}+\frac{ei_d}{\eta^2P^2}+\frac{e}{\eta P}+\frac{\lambda^2}{4c\Delta\lambda}}$$

where: λ – central light wavelength (1 550 nm), c – speed of light, D – loop diameter (0.25 m), L – loop length (about 6 000 m), k – Boltzmann's constant, T – temperature (293 K), R – resistance of the trans-impedance transducer of the photodetector device (20 kΩ), η – efficiency ratio of the photodiode (0.85 A/W), P – incident optical power on the APD, e – elementary charge, i_d – photodiode dark current (80 nA), $\Delta\lambda$ – spectral width of the light source (40 nm).

The calculated theoretical values of ARW for each optical head for four FORS type FOS6 were in the range of 4.49-4.85 nrad/√s, depending on total optical losses and fiber length in the given optical head.

Allan Variance analysis

Data gathered in the Military University of Technology, Poland

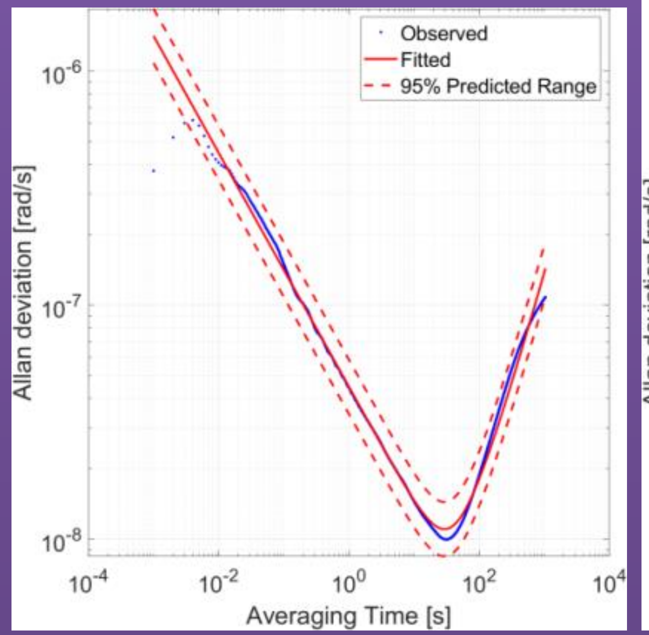

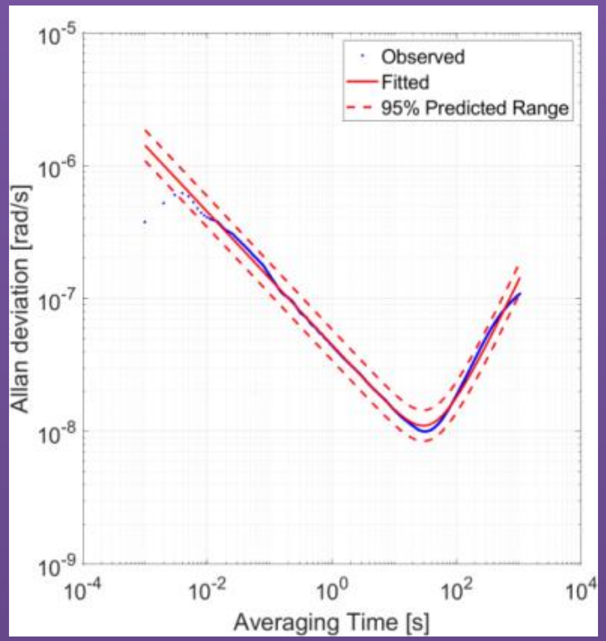

FOS6-01: ARW: 35 nrad/√s, BI: 10.0 nrad/s

FOS6-02: ARW: 45 nrad/√s, BI: 51.0 nrad/s https://fosrem.eu

FOSREM as FOS remote controls by webpage

System control

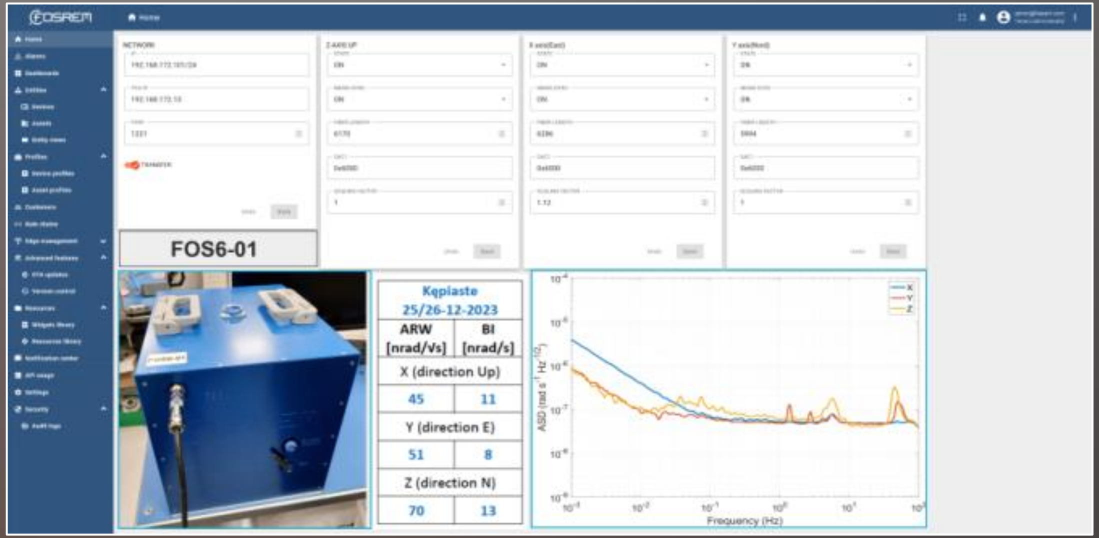

Paramters change

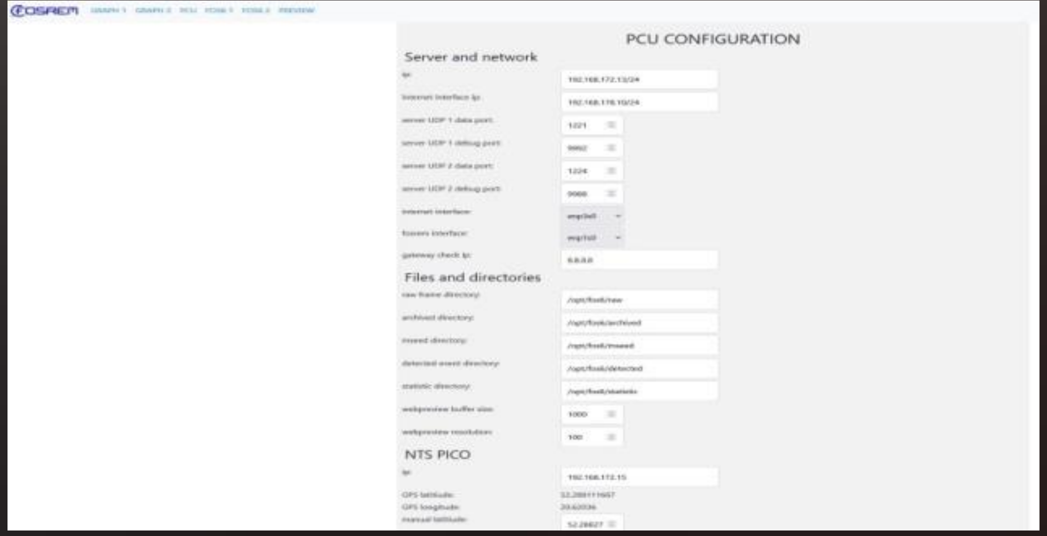

Data downloading

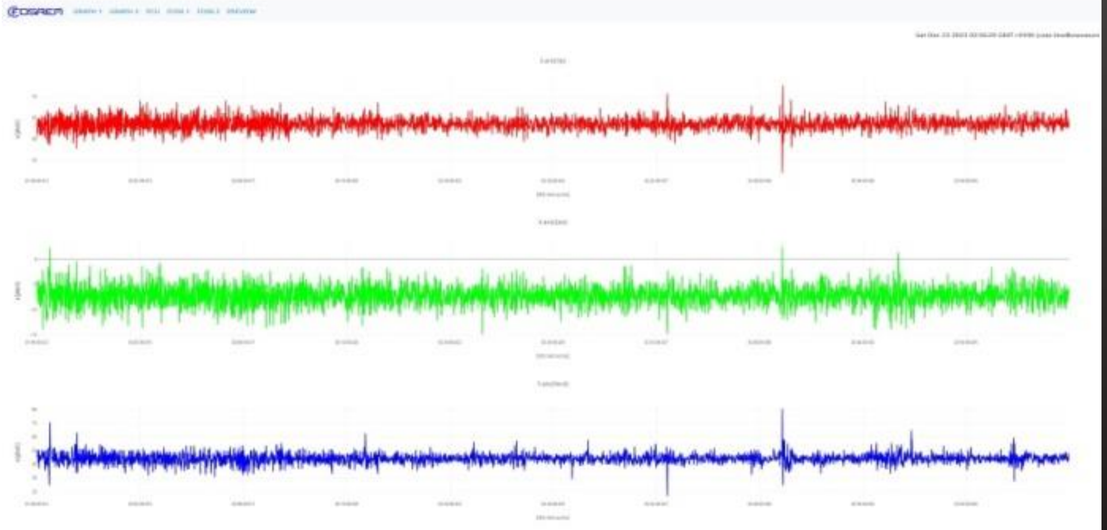

Localization

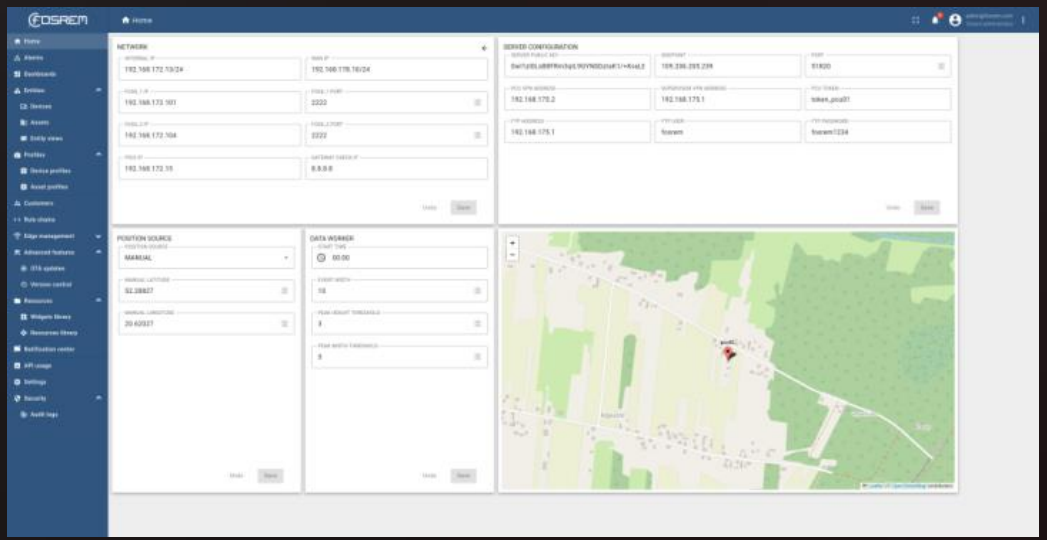

Correlation verification

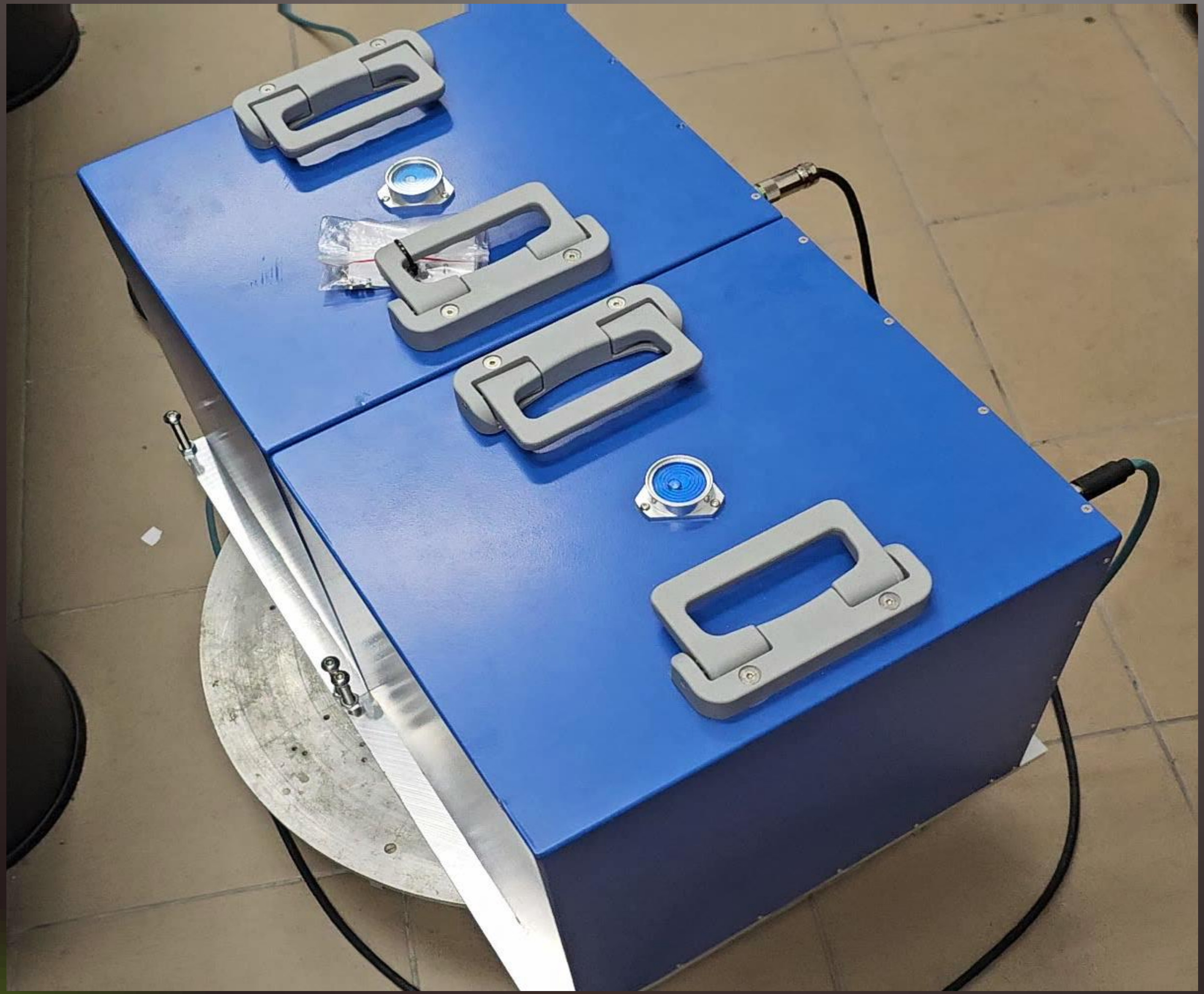

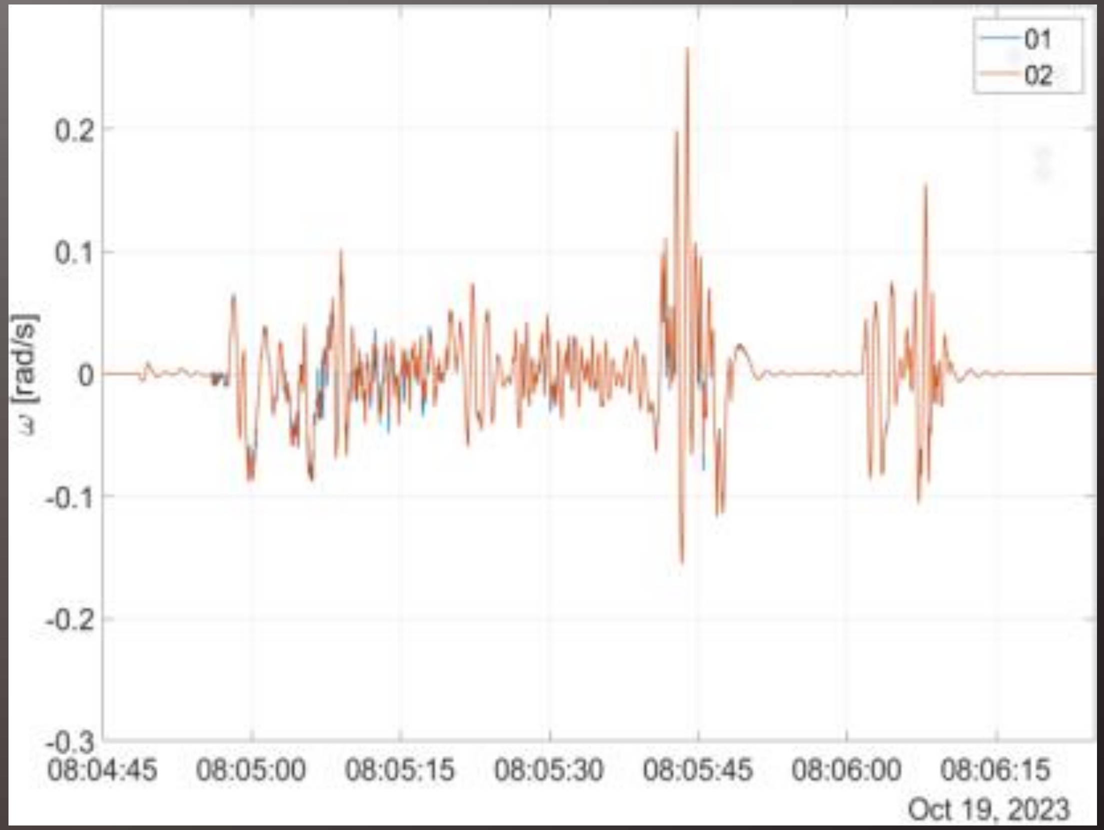

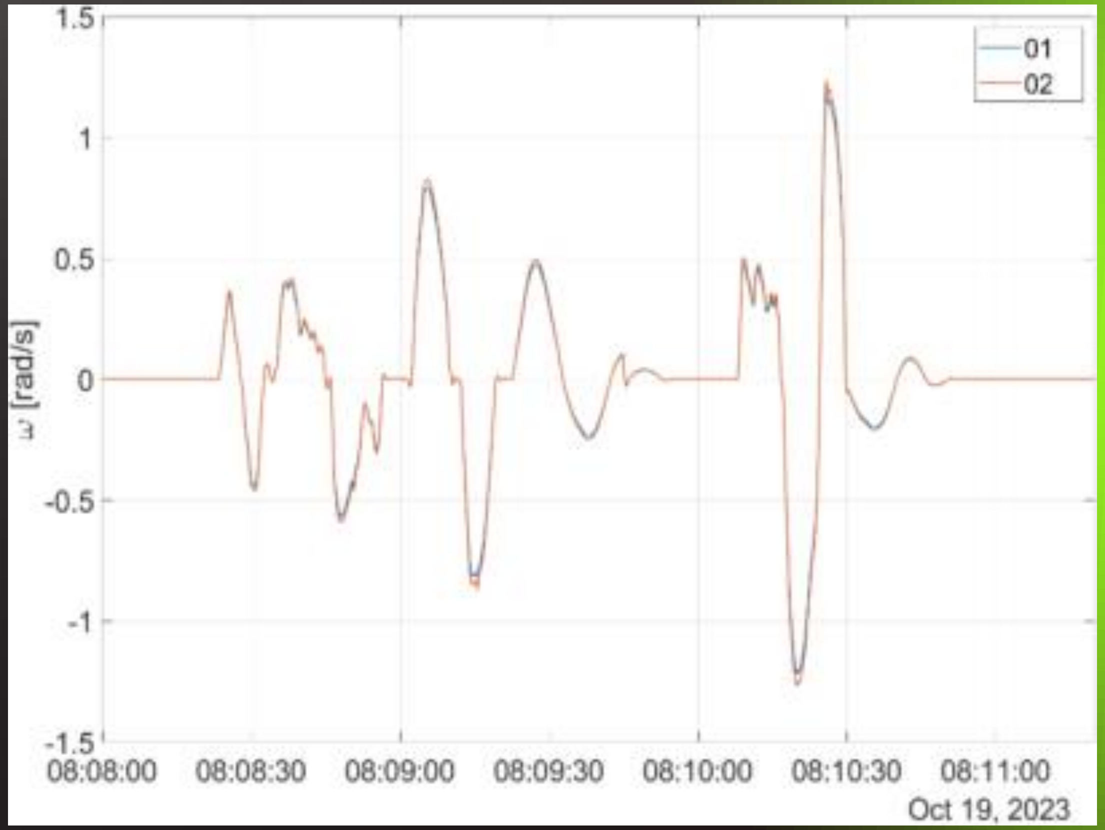

Signals recorded by FORSs Z-axes during the medium high-amplitude at a level of 0.25 rad/s and fast-changing excitations (at a level of 100 Hz) as well as high-amplitude at a level of 1.2 rad/s amplitude excitations

Pearson correlation coefficient equal to 99.42% and 99.99 %

Correlation verification

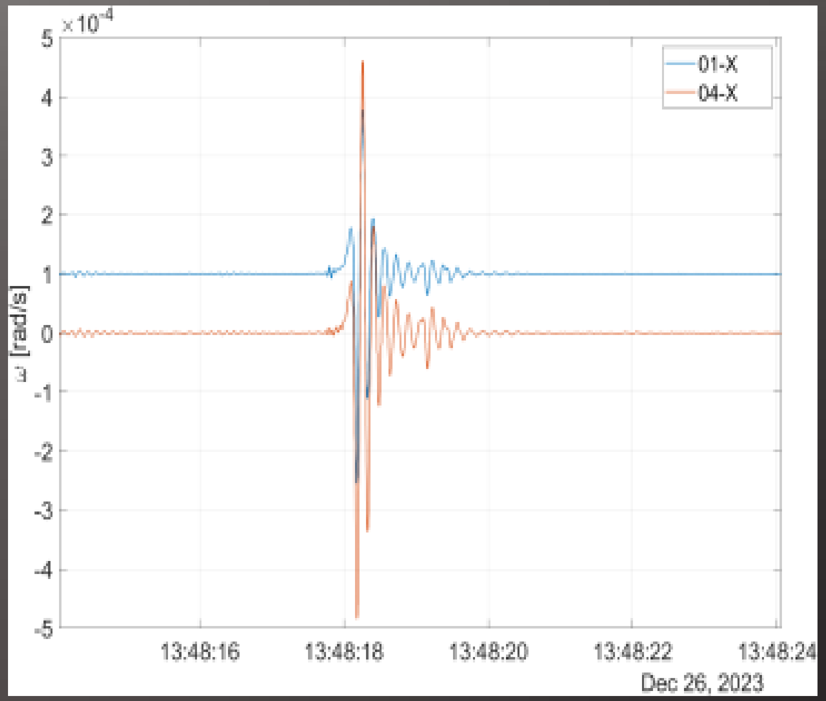

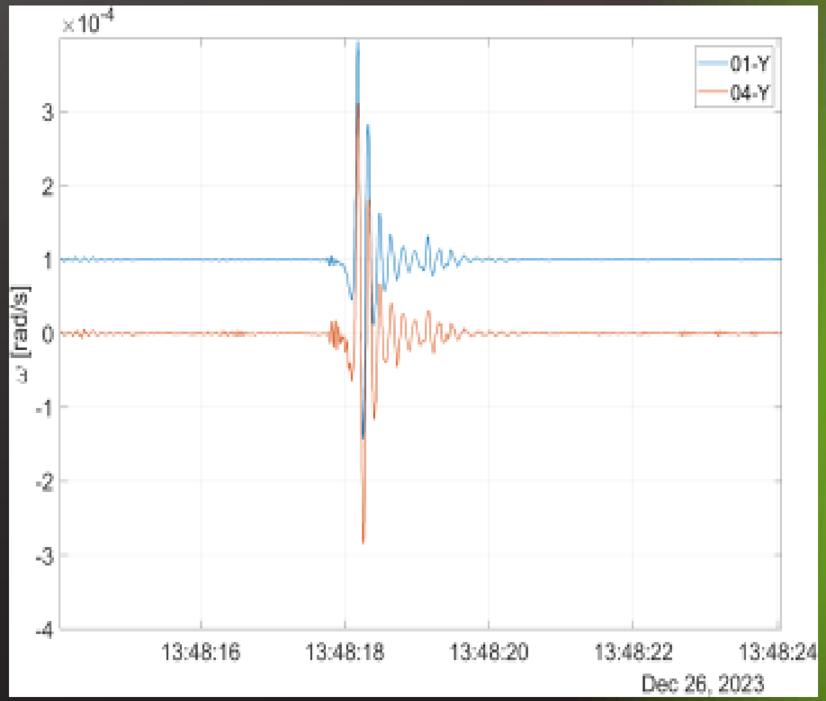

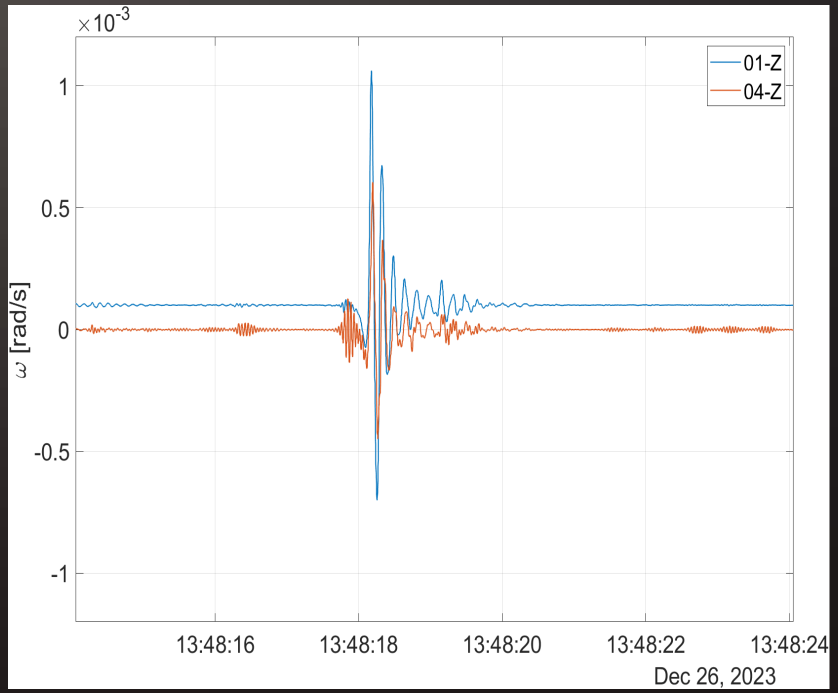

Field test in the Kampinos Nature Park by a pair of FORSs (FOS6-01 and FOS6-04)

A weak recording (with an amplitude of about 0.5 mrad/s)

Pearson correlation of about 95% for the X axis, about 99% for Y axis, and about 99% for the Z axis

Rotation Detection During Detonation of an Explosive Charge

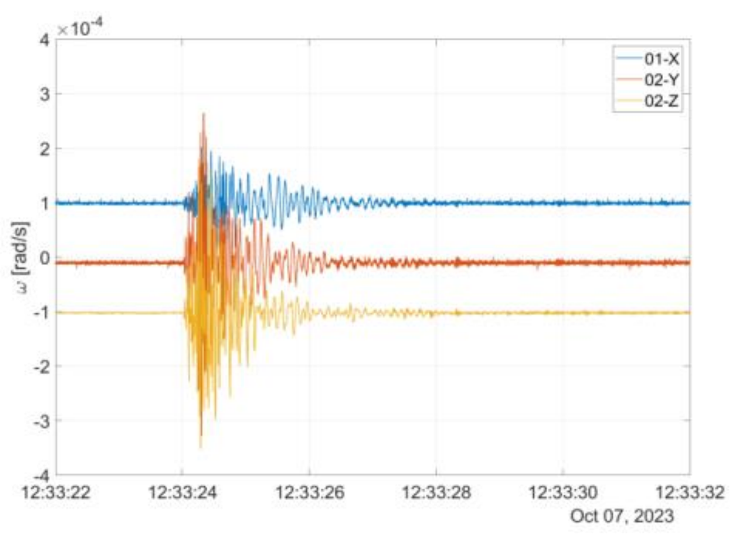

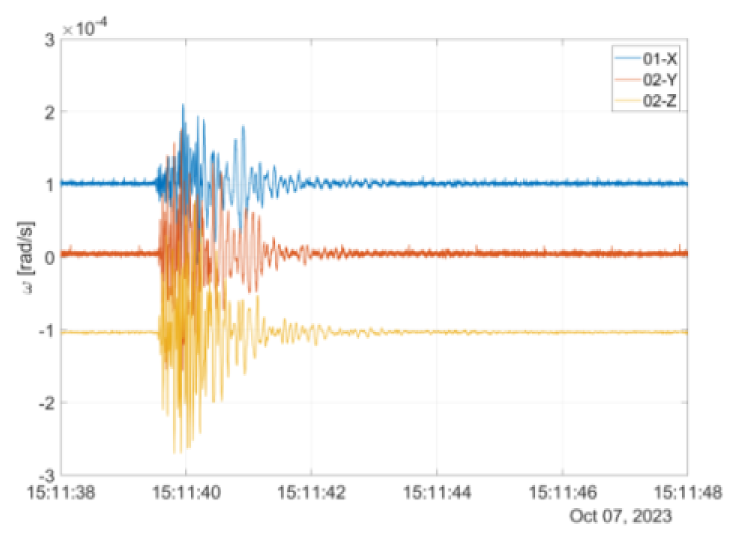

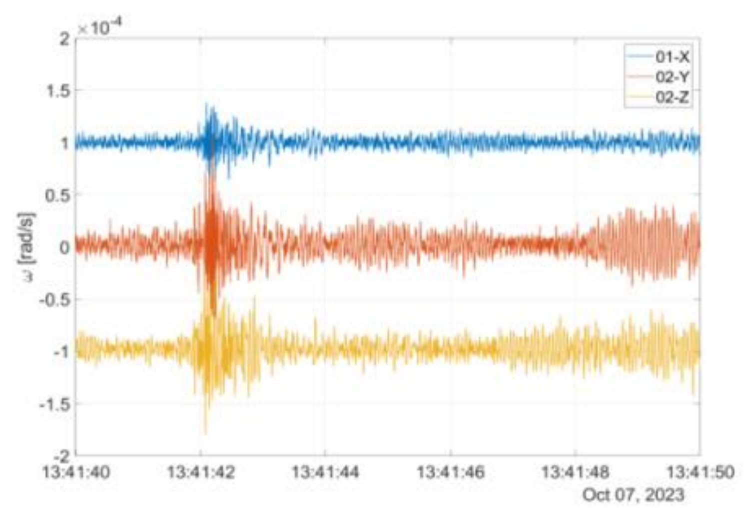

	A_{max} [μrad/s]			E_f [μrad]		
Explosion number/ Axis of FORS	X	Y	Z	X	Y	Z
Explosion 1	140	327	281	69	163	104
Explosion 2	38	108	83	41	98	94
Explosion 3	119	177	170	65	111	106

On the 7th of October 2023 there were three explosions performed:

1. 12:33 UTC, 5 kg of explosive, 3 m below the ground surface with surface discharge.
2. 13:41 UTC, 5 kg of explosive, 4.5 m below the ground surface without surface discharge.
3. 15:11 UTC, two 5 kg explosive charges installed 5 meters apart were detonated one after the other, 4.5 m below the ground surface, with a distance of 5 m between loads.

Conclusions

1 Data confirmed high reliability of recordings gathered by 3-axial Fibre-Optic Rotational Seismograph (correlation coefficient was near the value of 100%)

2 FORS recorded successfully artificial explosions in field test carried out in Szopowe, Poland which confirmed its usefulness of monitoring detonation tests, especially in border areas.

3 FORS main paramters:

- dynamics of 180 dB
- frequency detection bandpass: from 0.01 to 100 Hz
- built-in time scale synchronization system (accuracy 100ns)
- weight: less than 10 kg
- web-Based Management Interface
- possibility of mobile, autonomous operation

4 **Rotational seismology** undergoes a rapid development.

Future plans – 6 DoF recordings

Thank you very much for attention

Any questions?

You can find me at: anna.kurzych@wat.edu.pl

a.kurzych@elpromaelectronics.com

https://fosrem.eu/

Join us on 7th IWGoRS Meeting in Opole, Poland, 23-26 June, 2025

FOSREM - FROM SKY ACROSS GROUND UP TO UNDERGROUND

National Centre for Research and Development project POIR.01.01.01-00-1553/20-00

FOM-MEM - FIBRE-OPTIC MATRIX FOR MECHANICAL EVENTS MAPPING

Polish Agency for Enterprise Development project FENG.01.01-IP.02-1714/23